

RESEARCH ARTICLE

Distinct patterns of voxel- and connection-based white matter hyperintensity distribution and associated factors in early-onset and late-onset Alzheimer's disease

Hui Hong^{1,2}  | Yutong Chen² | Weiran Liu² | Xiao Luo¹ | Minming Zhang¹ | for the Alzheimer's Disease Neuroimaging Initiative (ADNI)

¹Department of Radiology, The Second Affiliated Hospital of Zhejiang University, School of Medicine, Hangzhou, China

²Department of Clinical Neurosciences, University of Cambridge, Cambridge, UK

Correspondence

Minming Zhang, MD PhD and Xiao Luo, PhD, Department of Radiology, The Second Affiliated Hospital of Zhejiang University, School of Medicine, Hangzhou, China. Email: zhangminming@zju.edu.cn and luoxiao1990@zju.edu.cn

Funding information

National Natural Science Foundation of China, Grant/Award Numbers: 81971577, 82271936

Abstract

Introduction: The distribution of voxel- and connection-based white matter hyperintensity (WMH) patterns in early-onset Alzheimer's disease (EOAD) and late-onset Alzheimer's disease (LOAD), as well as factors associated with these patterns, remain unclear.

Method: We analyzed the WMH distribution patterns in EOAD and LOAD at the voxel and connection levels, each compared with their age-matched cognitively unimpaired participants. Linear regression assessed the independent effects of amyloid and vascular risk factors on WMH distribution patterns in both groups.

Results: Patients with EOAD showed increased WMH burden in the posterior region at the voxel level, and in occipital region tracts and visual network at the connection level, compared to controls. LOAD exhibited extensive involvement across various brain areas in both levels. Amyloid accumulation was associated WMH distribution in the early-onset group, whereas the late-onset group demonstrated associations with both amyloid and vascular risk factors.

Discussion: EOAD showed posterior-focused WMH distribution pattern, whereas LOAD was with a wider distribution. Amyloid accumulation was associated with connection-based WMH patterns in both early-onset and late-onset groups, with additional independent effects of vascular risk factors in late-onset group.

KEYWORDS

early-onset Alzheimer's disease, late-onset Alzheimer's disease, white matter hyperintensities

Highlights

1. Both early-onset Alzheimer's disease (EOAD) and late-onset AD (LOAD) showed increased white matter hyperintensity (WMH) volume compared with their age-matched cognitively unimpaired participants.

Hui Hong and Yutong Chen contributed equally to this study.

This is an open access article under the terms of the [Creative Commons Attribution-NonCommercial-NoDerivs](https://creativecommons.org/licenses/by-nc-nd/4.0/) License, which permits use and distribution in any medium, provided the original work is properly cited, the use is non-commercial and no modifications or adaptations are made.

© 2024 The Authors. Alzheimer's & Dementia: Diagnosis, Assessment & Disease Monitoring published by Wiley Periodicals LLC on behalf of Alzheimer's Association.

2. EOAD and LOAD exhibited distinct patterns of WMH distribution, with EOAD showing a posterior-focused pattern and LOAD displaying a wider distribution across both voxel- and connection-based levels.
3. In both EOAD and LOAD, amyloid accumulation was associated with connection-based WMH patterns, with additional independent effects of vascular risk factors observed in LOAD.

1 | BACKGROUND

Early-onset Alzheimer's disease (EOAD) and late-onset AD (LOAD) are two subtypes of AD, based on an age cutoff of 65 years.¹ Both subtypes show amyloid and neurofibrillary tangles, with EOAD exhibiting a more widespread frontal and parietal distribution than LOAD.^{2,3} Regarding brain connectivity, EOAD tends to exhibit greater involvement of posterior white matter tracts and non-default mode networks,^{4,5} including those related to central executive function, language, working memory, and visuospatial processing. Moreover, clinically, EOAD often presents with more pronounced deficits in attention, executive function, and visuospatial ability relative to LOAD.^{4,6}

White matter hyperintensity (WMH), identified as hyperintense regions in T2 fluid-attenuated inversion recovery (T2-FLAIR) and T2-weighted magnetic resonance (MR) images,⁷ have been demonstrated to increase in volume in both EOAD and LOAD, and are associated with clinical symptom progression.^{8,9} However, the etiology of WMH in these two subtypes remains unclear. WMH in AD are often presumed to represent small-vessel ischemic brain injury due to underlying vascular risk factors including hypertension, diabetes, and hyperlipidemia.^{10,11} Nevertheless, a recent comprehensive review suggested that WMH in AD may have contributions beyond vascular factors,¹² and one community-based study demonstrated that vascular risk factors contribute to only 1% to 2% of WMH.¹³ Amyloid accumulation is recently suggested as another potential etiology for WMH.¹⁴⁻¹⁷ It has been hypothesized that amyloid could contribute to WMH via its connected tracts, a process known as Wallerian degeneration.¹²

One recent study involving both EOAD and LOAD cohorts suggested that increased WMH volume was related to amyloidosis rather than to vascular risk factors.¹⁸ However, this study did not investigate the association with WMH distribution at the voxel level. It is worth noting that previous voxel-based WMH studies found that WMH in different regions were associated with divergent etiologies, with periventricular WMH linked to vascular risk factors,¹⁹⁻²¹ whereas amyloid accumulation was found to be more associated with posterior WMH distribution.^{16,22} In addition, the connection-based mechanism between amyloid accumulation and WMH suggests that the distribution of WMH in AD may follow a pattern based on connections within the brain. This could be assessed by analyzing the streamlines passing through WMH lesions and examining the connectivity between cortical regions that are disrupted by these lesions. Previous studies have

utilized similar methods to evaluate the impact of other lesions, such as stroke or tumors, on brain connectivity.^{23,24} However, so far, no study has investigated the connection-based WMH distribution pattern in EOAD and LOAD.

Therefore, in this study, we aim to investigate distribution patterns of WMH at both the voxel- and connection-based levels in both EOAD and LOAD. In addition, we will explore the factors, including amyloid and vascular risk factors, associated with WMH distribution patterns in both the early-onset and late-onset groups. We hypothesize that EOAD may exhibit more restricted WMH distribution patterns. Furthermore, we anticipate that the WMH distribution patterns in EOAD and LOAD will be associated with different factors, with vascular risk factors playing a greater role in LOAD.

2 | METHODS

2.1 | Participants

We downloaded the study data from the Alzheimer's Disease Neuroimaging Initiative (ADNI) publicly available database before July 2023. Each participant underwent MRI scanning and neuropsychological evaluations, with some completing amyloid positron emission tomography (PET) scanning and phosphorylated tau 181 (p-tau181) plasma assessment. All participants completed the Mini-Mental State Examination (MMSE) and Clinical Dementia Scale Sum of Boxes (CDR-SB) to assess general cognitive ability and dementia severity, respectively. Neurologists from multiple sites made the AD diagnosis. We divided AD patients into EOAD and LOAD groups (age <65 years and ≥65 years, respectively). Age-matched cognitive unimpaired participants were also included. The criteria for cognitive unimpaired participants are shown in Supplementary Method 1.

2.2 | Vascular risk factors

Vascular risk factors, including hypertension, diabetes, hyperlipidemia, smoking, history of ischemic heart disease, and history of stroke, were recorded as presence (1) or absence (0), according to past medical histories of each participant in ADNI1, ADNI2, and ADNI3. Detailed searching methods were provided in Supplementary Method 2.

2.3 | MRI acquisition

Each participant underwent a 3T MRI scan with the T1-weighted structural imaging sequence utilized an inverse recovery spoiled gradient recall (IR-SPGR) protocol, and T2 FLAIR data, which consisted of two main types, namely axial T2-FLAIR and sagittal three-dimensional (3D) FLAIR. The acquisition parameters were provided in Supplementary Method 3.

2.4 | Amyloid PET

Amyloid beta ($A\beta$) PET scans were conducted using two radiotracers (florbetapir or florbetaben). The PET data underwent correction using the ADNI PET processing pipeline, as outlined previously²¹; the detailed processing steps were included in Supplementary Method 4. In an effort to advance the harmonization of $A\beta$ PET, we employed data from [¹⁸F]florbetaben (FBB) and [¹⁸F]florbetapir (FBP) to generate (1) standardized Centiloid (CL) conversions as described previously.²⁵ In the subsequent sections of this article, we use CL to represent the relative levels of amyloid.

2.5 | Image preprocessing

N4 bias correction was applied on the T1 and FLAIR images using the Advanced Normalization Tools (ANTs) package.²⁶ T1 images were skullstripped using HD-BET.²⁷ Skullstripped T1 images were segmented by FreeSurfer to obtain total brain volume and white matter volume.²⁸ Skullstripped T1 images were registered to the Montreal Neurological Institute (MNI) template using rigid registration. The resulting transform was used to register FLAIR to the template. In the MNI space, WMH lesions were segmented using HyperMapper.²⁹ Segmentation results were manually corrected by three experienced clinicians. Infratentorial WMH segmentations were manually deleted.

T1 images were registered to the MNI template using symmetric normalization in the ANTs package. To correct for ventricular shape, white matter (WM) was segmented from the T1 images and MNI template using the FAST function from FMRIB Software Library (FSL).³⁰ WM from T1 was registered to the WM mask of the MNI space using symmetric normalization. The same transformation was used to warp the WMH mask.

2.5.1 | Quantification of WMH burden in tracts

For each participant, the tractogram template from the Human Connectome Project³¹ was superimposed onto the WMH mask in the MNI space. The burden of WMH in a WM tract was defined as the number of streamlines passing through WMH lesions in the tract (Figure 1).²³ This was calculated for each of the 66 WM tracts in the tractogram template. The higher number of streamlines passing through WMH lesions indicates a more severe burden of WMH in specific tract, as shown in Figure 1.

RESEARCH IN CONTEXT

- 1. Systematic Review:** Increased white matter hyperintensity (WMH) volume is shown in both early-onset Alzheimer's disease (EOAD) and late-onset AD (LOAD). With searching of common literature review resources such as PubMed, we found a discussion on the factors associated with WMH in AD; however, we did not identify a comprehensive study on the factors associated with WMH distribution pattern in EOAD and LOAD separately.
- 2. Interpretation:** In our study, we present a comprehensive analysis of the WMH distribution pattern in both voxel- and connection-based levels. Our findings demonstrated that EOAD displayed a more restricted pattern of WMH distribution, likely attributed to amyloid accumulation. Conversely, LOAD showed more widespread WMH distribution patterns, which were associated with both amyloid and vascular risk factors. Our study indicates the potential need for different treatment approaches to WMH in EOAD and LOAD.
- 3. Future Directions:** Longitudinal changes in voxel- and connection-based WMH distribution patterns and their related factors are needed to further illustrate the mechanism underlying WMH progression in EOAD and LOAD.

2.5.2 | Quantification of WMH burden in brain networks

The cortex was parcellated into 78 regions using the Human Connectome Project Multimodal parcellation atlas.³² The connectivity between any two regions is defined as the number of streamlines that connected both cortical regions and passed through WMH lesions. Whole brain global efficiency was used to quantify whole brain global connectivity. Higher global efficiency indicates a more severe burden of WMH in the network (Figure 1).

WMH burden was also quantified in each subnetwork (default mode, frontoparietal, ventral attention, dorsal attention, somatomotor, visual, and limbic networks) as defined in the Yeo network atlas³³ (Figure 1), by including only the subnetwork-specific cortical regions in calculating global efficiency.

2.6 | Statistics

For demographics, amyloid level, and vascular risk factors, the Shapiro-Wilk test was performed to assess normality. If the variable was normally distributed, we summarized it using the mean and standard deviation (SD). For variables not normally distributed, median and interquartile range were used. To compare the difference in contin-

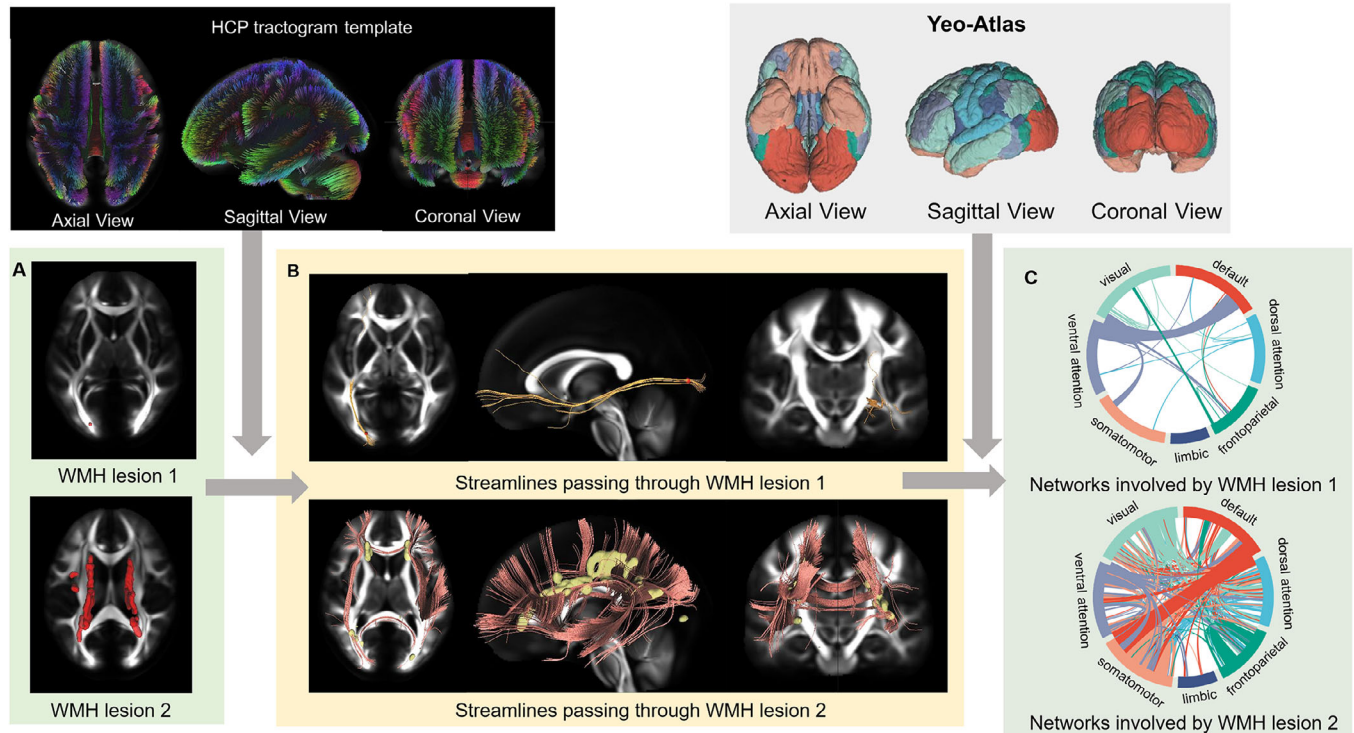


FIGURE 1 The workflow of connection-based white matter hyperintensity (WMH) distribution analysis. (A) WMH distribution (top: participants with minor WMH, bottom: participants with severe WMH). (B) Streamlines passing through WMH lesion. (C) Networks involved by WMH lesions.

ous variables between AD patients and the age-matched cognitive unimpaired participants, the independent *t*-test was used for normally distributed variables and the Wilcoxon rank-sum test was for non-normally distributed variables. The chi-square test was performed for binary variables.

2.6.1 | Comparing voxel- and connection-based WMH distribution in EOAD and LOAD with the age-matched cognitively unimpaired participants

For voxel-based WMH distribution analysis, we used the voxel-based lesion symptom mapping (VLSM) method; only the voxels covered by WMH lesions in at least 2.5% of the cohort were selected. Logistic regression was conducted between the presence of WMH lesion and the diagnosis of AD within these voxels, with age and sex included as covariates. *p*-values were adjusted using the Benjamini–Hochberg method across all tested voxels.

For the analysis of WMH burden in tracts, linear regression was used to assess the group streamlines difference in each tract, with age and sex being the covariates and the diagnosis of AD being the independent variable. The dependent variable was the streamline number passing through WMH lesions in a tract. *p*-Values were adjusted using Benjamini–Hochberg method across all tracts.

To summarize, the WMH burden across all the WM tracts, principal component analysis (PCA) was performed on the number of

streamlines passing through WMH lesions in each WM tract across all participants in either the EOAD group or the LOAD group (EOAD and LOAD and their age-matched cognition unimpaired participants). The first principal component (PC1) served as the summary metric, with the positive end representing participants with more WMH lesions in the white matter tracts. We performed a linear regression using PC1 as the dependent variable, with age and sex as covariates, and the diagnosis of AD as the independent variable.

For the analysis of WMH burden in brain networks, linear regression models were employed to explore group differences in network global efficiency, with age and sex as covariates and the diagnosis of AD as the independent variable. Both whole brain global efficiency and each subnetwork global efficiency were sequentially entered as dependent variables. *p*-Values were adjusted for multiple comparisons across different network modules using the Benjamini–Hochberg method.

Each of the analyses (VLSM, WMH burden in each tract, PC1 of streamlines passing through WMH in each tract, and WMH burden in brain networks) was repeated to investigate the differences between EOAD and LOAD. For VLSM analysis, a chi-square test was performed between the presence of the WMH lesion and the diagnosis of AD within these voxels. *p*-Values were adjusted using the Benjamini–Hochberg method across all tested voxels. For WMH burden in each tract, PC1 of streamlines passing through WMH in each tract and WMH burden in brain networks, Shapiro–Wilk test was used to assess normality. An independent *t*-test was performed between for normally distributed variables and Wilcoxon rank-sum test was

TABLE 1 Demographic characteristics.

	YCU (n = 55)	EOAD (n = 65)	p	ECU (n = 162)	LOAD (n = 212)	p
Age, median (IQR)	61.2 (57.5–63.2)	61.9 (58.6–63.9)	0.254	76.8 (73.1–81.9)	77.3 (73.8–81.3)	0.799
Sex (male), n (%)	16 (29.1)	23 (35.4)	0.591	83 (51.2)	126 (59.4)	0.140
Education (years), median (IQR)	16.0 (14.0–18.0)	16.0 (14.0–18.0)	0.996	17.0 (16.0–18.0)	16.0 (14.0–18.0)	0.002
APOE ε4 status						
APOE ε4+, n (%)	11 (20.0)	46 (70.8)	0.001	35 (21.6)	150 (70.8)	<0.001
APOE ε4–, n (%)	21 (38.2)	17 (26.2)	0.225	127 (78.4)	59 (27.8)	<0.001
No genetics data, n (%)	23 (41.8)	2 (3.1)	<0.001	0 (0)	3 (1.4)	0.350
Vascular risk factors						
Diabetes, n (%)	4 (7.4)	6 (9.4)	0.960	13 (8.0)	19 (9.0)	0.893
Hypertension, n (%)	17 (31.5)	15 (23.4)	0.440	64 (39.5)	92 (43.4)	0.516
Hyperlipidemia, n (%)	16 (29.6)	20 (31.2)	1.000	68 (42.0)	105 (49.5)	0.178
IHD, n (%)	0 (0)	1 (1.6)	1.000	10 (6.2)	22 (10.4)	0.210
Stroke, n (%)	0 (0)	1 (1.6)	1.000	0 (0)	2 (0.9)	0.600
Smoking, n (%)	3 (5.6)	3 (4.7)	1.000	21 (13.0)	27 (12.7)	1.000
Amyloid, median (IQR)	7.4 (0.9–11.4)	76.9 (47.3–99.1)	<0.001	3.0 (–3.1–9.4)	81.6 (58.6–104.3)	<0.001
WMH volume (mL), median (IQR)	1.8 (0.7–2.6)	3.2 (1.7–5.7)	<0.001	4.1 (2.1–9.4)	8.7 (4.4–16.0)	<0.001

Abbreviations: APOE, apolipoprotein E gene; YCU, young cognitively unimpaired; EOAD, early-onset Alzheimer's disease; ECU, elderly cognitively unimpaired; LOAD, late-onset Alzheimer's disease; IHD, ischemic heart disease; IQR, interquartile range, WMH, white matter hyperintensity.

used for non-normally distributed variables to compare the difference between EOAD and LOAD.

2.6.2 | The influence of amyloid and vascular risk factors on voxel- and connection-based WMH distribution patterns in the early-onset group and late-onset group

The analyses of factors associated with voxel- and connection-based WMH distribution were carried out in the early-onset group (including EOAD and its age-matched cognitive unimpaired participants) and late-onset group (including LOAD and its age-matched cognitive unimpaired participants) separately. This separation was performed considering that AD development is a chronic, continuous process.

History of stroke in both groups and history of ischemic heart disease (IHD) in the early-onset group were not analyzed due to their low prevalence rate (Table 1).

VLSM was conducted with the same design as described. Logistic regression was performed with the presence or absence of WMHs as the dependent variable. Independent variables included age, sex, amyloid levels, vascular risk factors such as hypertension, diabetes, hyperlipidemia, smoking, and history of IHD. *p*-Values were adjusted using the Benjamini–Hochberg method across all tested voxels.

For analysis of factors associated with WMH burden in tracts a linear regression analysis was conducted with age, sex, vascular risk factors, and amyloid levels as independent variables. PC1 of streamlines passing through WMHs in each tract was specified as the dependent variable.

Linear regression analyses were also performed for factors associated with WMH burden in each network. Age, sex, vascular risk factors, and amyloid levels were included as independent variables. Whole brain global efficiency and each subnetwork global efficiency were entered as dependent variables sequentially.

A separate analysis was performed on the entire cohort (early and late onset) with the inclusion of an interaction term between age and amyloid level to investigate if the effect of amyloid on voxel-based WMH distribution, the PC1 of streamlines passing through WMH in each tract, and global efficiency in each network could be moderated by age.

2.7 | Software

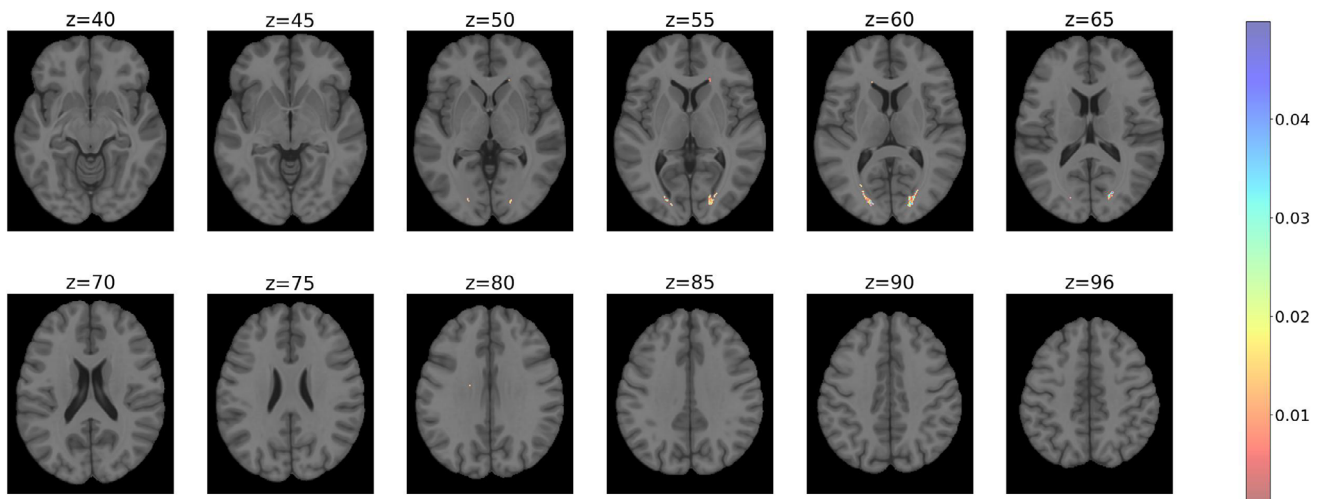
Image preprocessing was implemented in python 3.8.6. Voxel-based lesion symptom mapping was implemented in Julia 1.9.0. WMH connectivity analysis was conducted using Fortran 90 subroutines that were translated from the Brain Connectivity Toolbox.²⁷ All statistical analyses were performed in R version 4.2.0. The analysis scripts are available: <https://github.com/Yutong441/ADcon>.

3 | RESULTS

3.1 | Cohort selection

Fifty-five young cognitively unimpaired (YCU), 65 EOAD, 162 elderly cognitively unimpaired (ECU), and 212 LOAD were included

Early onset group



Late onset group

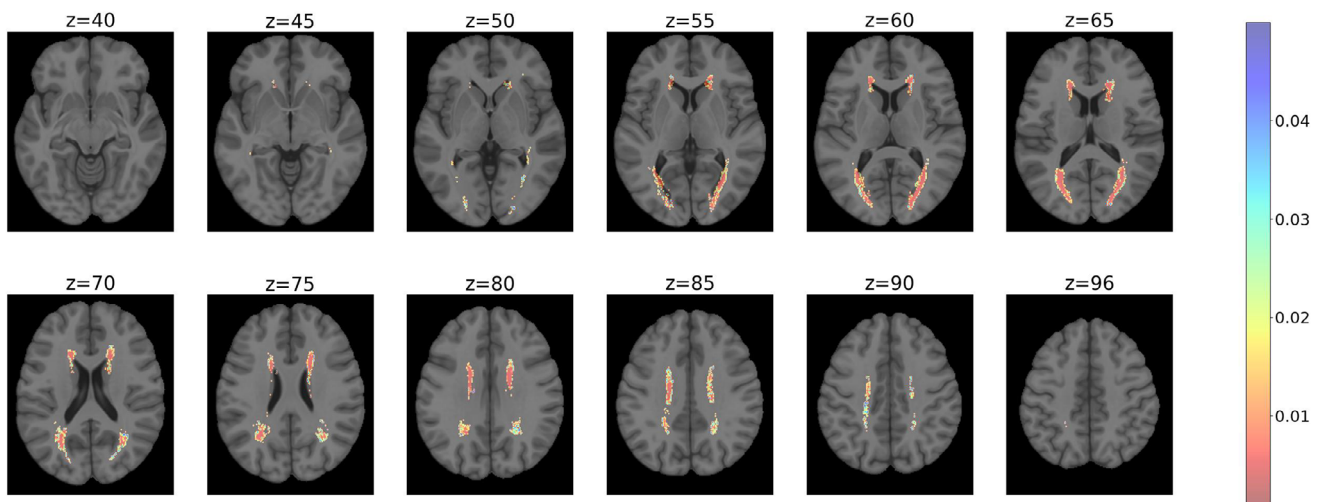


FIGURE 2 Comparison of voxel-based white matter hyperintensity (WMH) distribution in early-onset Alzheimer's disease (EOAD; top panel) and late-onset AD (LOAD; bottom panel) with age-matched cognitively unimpaired participants.

(Figure S1). There was no difference in age and sex between YCU (age: 61.2[57.5-63.2], male: 29.1%) and EOAD (age:61.9 [58.6-63.9], male: 35.4%), and ECU (age: 76.8[73.1-81.9], male: 51.2%) and LOAD (age: 77.3 [73.8-81.3], male: 59.4%) (Table 1). Both EOAD (3.2 [1.7-5.7] ml vs 1.8 [0.7-2.6] ml, $p < 0.001$) and LOAD (8.7[4.4-16.0] ml vs. 4.1 [2.1-9.4] ml, $p < 0.001$) showed significantly increased WMH volume compared with the age-matched cognitively unimpaired participants. Other comparison results were shown in Table 1.

3.2 | Distinguishing voxel- and connection-based WMH distribution patterns in EOAD and LOAD compared to age-matched cognitively unimpaired participants

For VLSM analysis, we found that EOAD and LOAD patients have similar patterns of voxel-based WMH distribution (Figure S2), most

prominently in the periventricular regions and posterior region. Both EOAD and LOAD showed increased WMH burden in posterior region bilaterally compared with the age-matched cognitively unimpaired participants, after adjusting for age and sex (Figure 2). In LOAD, more significant voxels were identified in the periventricular region in the frontal lobe (Figure 2).

For analysis of WMH burden in tracts, we found that both EOAD and LOAD showed significantly different PC1 of streamlines passing through WMH in each tract compared to their age-matched normal controls (Table 2). Detailed differences of tracts passing through WMH were shown in Figure 3. Compared with age-matched cognitively unimpaired participants, EOAD patients displayed significantly higher WMH burden in the tracts located at the occipital region (Figure 3), including the optic radiation bilaterally, anterior commissure, and inferior fronto-occipital fasciculus (Table S1). LOAD patients demonstrated a more widespread WMH burden among different tracts (Figure 4). More details of the involved tracts were shown in Table S2.

TABLE 2 Comparison of networks global efficiency and PC1 of streamlines passing through WMH lesion in each tract in EOAD and LOAD with the age-matched cognitively unimpaired participants.

	Early onset	Late onset
Network global efficiency		
Whole brain	0.41	0.56***
Default mode	0.17	0.39***
Frontoparietal	0.18	0.48***
Ventral attention	0.27	-0.10
Dorsal attention	0.33	0.31**
Somatomotor	0.40	0.50***
Visual	0.81***	0.67***
Limbic	-0.30	-0.31**
Streamlines		
PC1	0.20*	0.23***

Note: Adjusted for age and sex.

*** indicates p -value < 0.001; ** indicates p -value from 0.001 to 0.01; * indicates p -value from 0.01 to 0.05; indicates p -value from 0.05 to 0.1.

Abbreviations: PC1, first principle component.

For WMH burden in the brain network analysis, EOAD patients exhibited significantly higher global efficiency in visual networks compared to the age-matched cognitive unimpaired participants (Table 2). LOAD patients showed significantly higher global efficiency in whole brain, default mode, frontoparietal, dorsal attention, somatomotor, and visual network global efficiency (Table 2), but displayed a lower global efficiency in the limbic network compared to age-matched normal participants.

For comparison between EOAD and LOAD, we observed that in LOAD, more significant voxels were identified in the periventricular region and posterior region compared to EOAD (Figure S3). Regarding the analysis of WMH burden in tracts, we found that LOAD exhibited severe WMH burden in tracts compared to EOAD, as reflected by PC1 of streamlines passing through WMHs in each tract (EOAD: -10.33 [-13.50 to -47.53] vs LOAD: 13.49 [77.48-115.44]) (Table S3). In the WMH burden in brain network analysis, LOAD patients displayed significantly higher global efficiency in whole brain, default mode, frontoparietal, dorsal attention, somatomotor, and visual networks. Conversely, EOAD patients exhibited a significantly higher global efficiency in the ventral attention network (Table S3).

3.3 | Effects of amyloid and vascular risk factors on voxel- and connection-based WMH distribution in the early-onset group and late-onset group

In our voxel-based WMH distribution analysis, we observed no effect of amyloid and vascular risk factors on WMH distribution in the early-onset group. However, in the late-onset group, we found that the presence of pathologically defined amyloid levels, hypertension, and smoking was associated with the WMH burden in the brain, as

illustrated in Figure 4. Specifically, hypertension was associated with increased WMH burden in the anterior horn of the lateral ventricle, whereas smoking and pathologically defined amyloid levels were related to more widespread WMH (Figure 4).

For WMH burden in tracts analysis, PC1 streamlines passing through WMH in each tract was significantly associated with only amyloid ($\beta = 0.19$) in the early-onset group; however, for the late-onset group PC1 was significantly associated with amyloid ($\beta = 0.19$), hypertension ($\beta = 0.18$), and smoking ($\beta = 0.16$) (Table 3).

For WMHs in the connected network analysis, we found that amyloid was positively associated with whole brain global efficiency in both the early-onset group ($\beta = 0.20$) and late-onset group ($\beta = 0.25$). In addition, hypertension ($\beta = 0.16$) and smoking ($\beta = 0.18$) were positively associated with whole brain global efficiency in the late-onset group. For subnetwork global efficiency analysis, we found that amyloid was positively associated with only visual network global efficiency ($\beta = 0.32$) in early-onset group. In the late-onset group, we found that hypertension was positively associated with fronto-parietal ($\beta = 0.19$), limbic ($\beta = 0.12$), somatomotor ($\beta = 0.12$), and visual network ($\beta = 0.11$) global efficiency, and that smoking was positively associated with default ($\beta = 0.22$), dorsal attention ($\beta = 0.14$), fronto-parietal ($\beta = 0.14$), and visual network ($\beta = 0.13$) global efficiency. However, we found that hypertension was negatively associated with ventral attention network global efficiency in both the early-onset ($\beta = -0.27$) and late onset groups ($\beta = -0.12$) (Table 4).

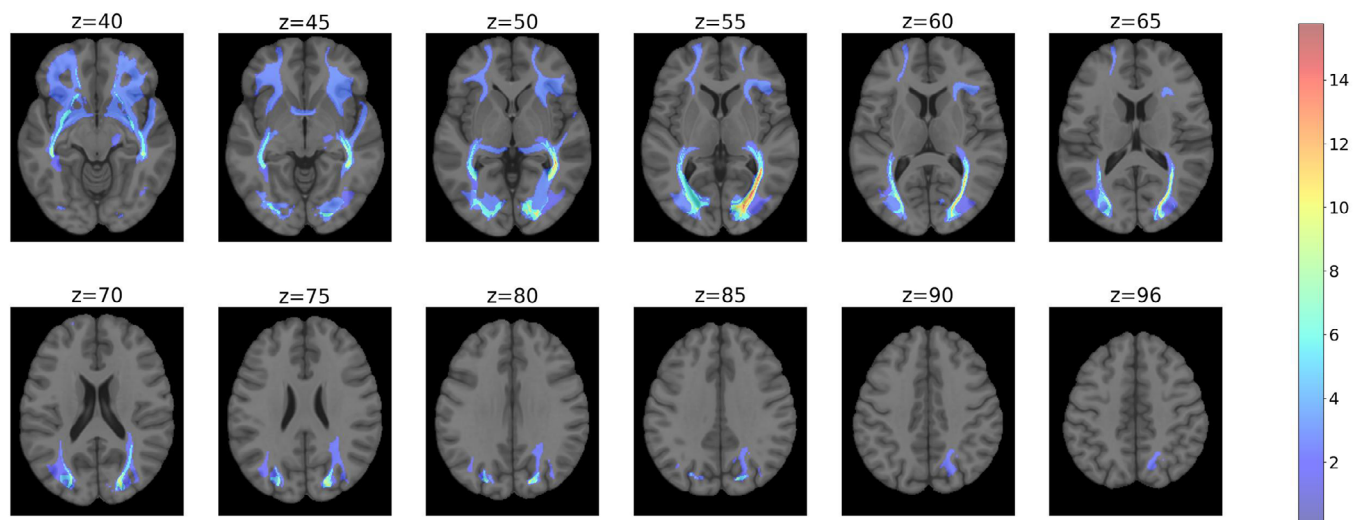
In the whole cohort analysis, we did not find the significance of age*amyloid in voxel- and connection-based WMH distribution (Tables S4 and S5).

4 | DISCUSSION

We have analyzed WMH distribution patterns in EOAD and LOAD patients at voxel- and connection-based levels. In EOAD patients, WMH was confined in posterior region tracts and in visual network, whereas in LOAD, WMH had a broader distribution among multiple tracts and networks. In both the early-onset and late-onset groups, connection-based WMH distribution patterns were associated with amyloid burden, and in the late-onset group, vascular risk factors had an additional independent effect on voxel- and connection-based WMH patterns.

The observation that amyloid was associated with connection-based WMH distribution patterns, including higher WMH burden in tracts and networks, in both EOAD and LOAD suggested that amyloid could contribute to the WMH presence in tracts or networks. Previous studies have also demonstrated similar findings, indicating that regional amyloid accumulation in cortical regions could lead to appearance of WMHs in connected tracts.³⁴⁻³⁶ Wallen degeneration, triggered by amyloid accumulation in cortical regions, could damage their connected tracts, subsequently resulting in the presence of WMHs. This type of WMH is more closely related to secondary degeneration followed AD pathologies. However, we did not find significant age*amyloid interaction effect on connection-based WMH

Early onset group



Late onset group

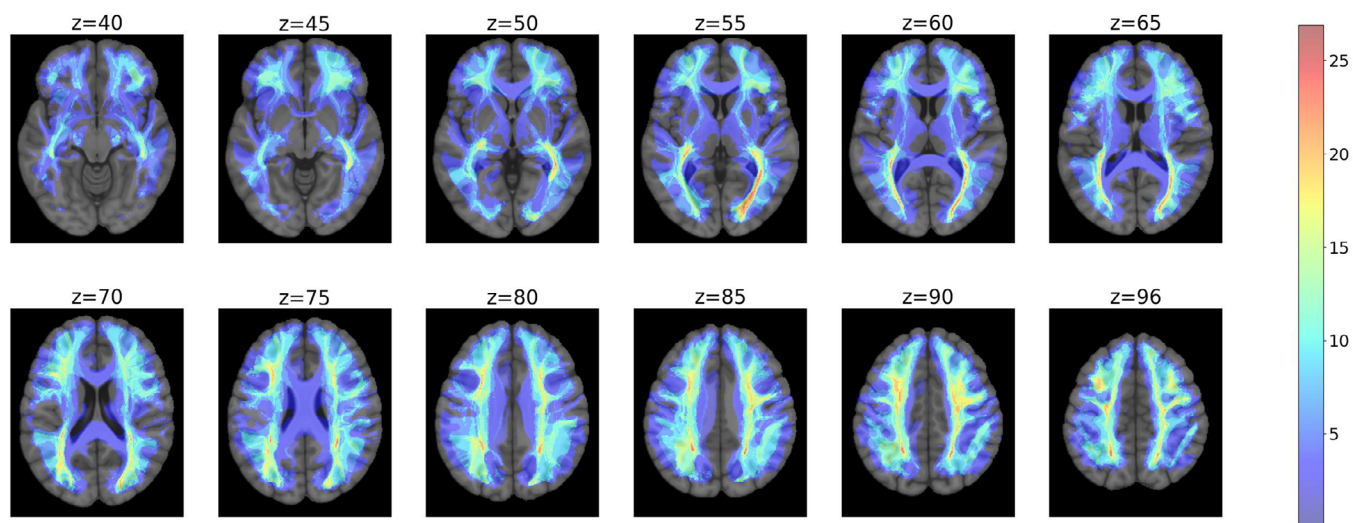


FIGURE 3 Comparison of white matter hyperintensity (WMH) burden in tracts in early-onset Alzheimer's disease (EOAD; top panel) and late-onset AD (LOAD; bottom panel) with age-matched cognitively unimpaired participants. Note: Only voxels with $p < 0.05$ were shown.

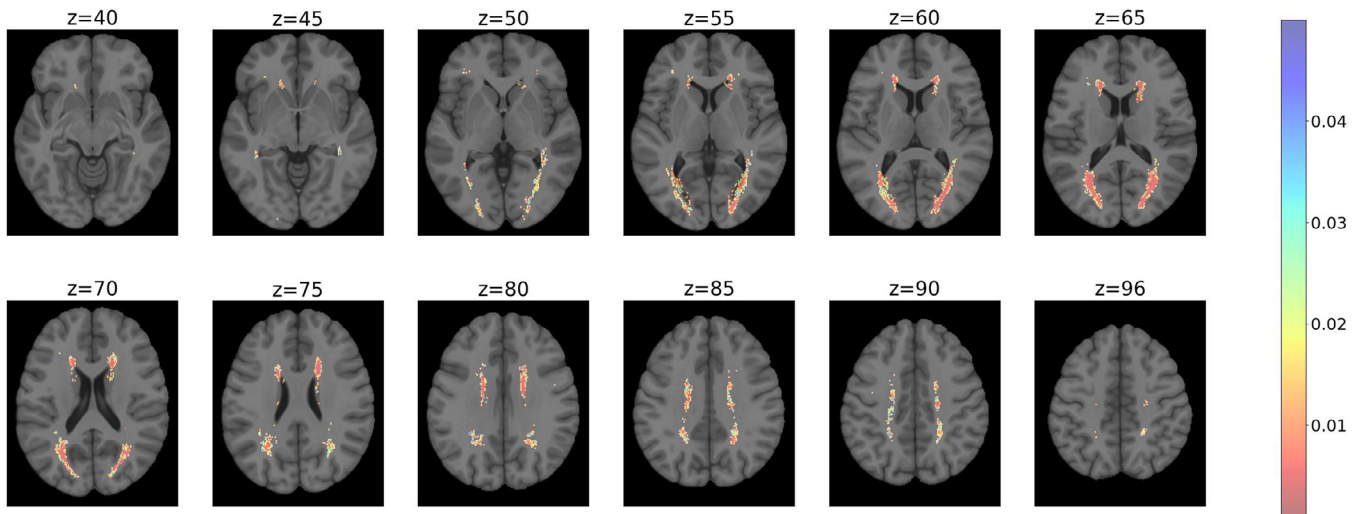
patterns, indicating that there is no difference in the amyloid effect on connection-based WMH burden in EOAD and LOAD.

Apart from the effect of amyloid, hypertension and smoking were associated with increased voxel- and connection-based WMH burden in LOAD. The voxel-based pattern associated with hypertension mainly located in periventricular regions, which is consistent with a previous study analyzing voxel-based distribution of WMHs in older communities.²⁰ We did not find the association between vascular risk factors and voxel-based and most of connection-based WMH distribution patterns in EOAD. This indicated that WMHs in LOAD have multiple etiologies compared to those in EOAD. In LOAD, aging itself, and also a higher prevalence of vascular risk factors are all risk factors for vascular-related increased WMH volume.^{37,38} However, for WMH burden in connection networks, we found that hypertension was negatively associated with global efficiency in the ventral network. The ventral network is connected by tracts passing through

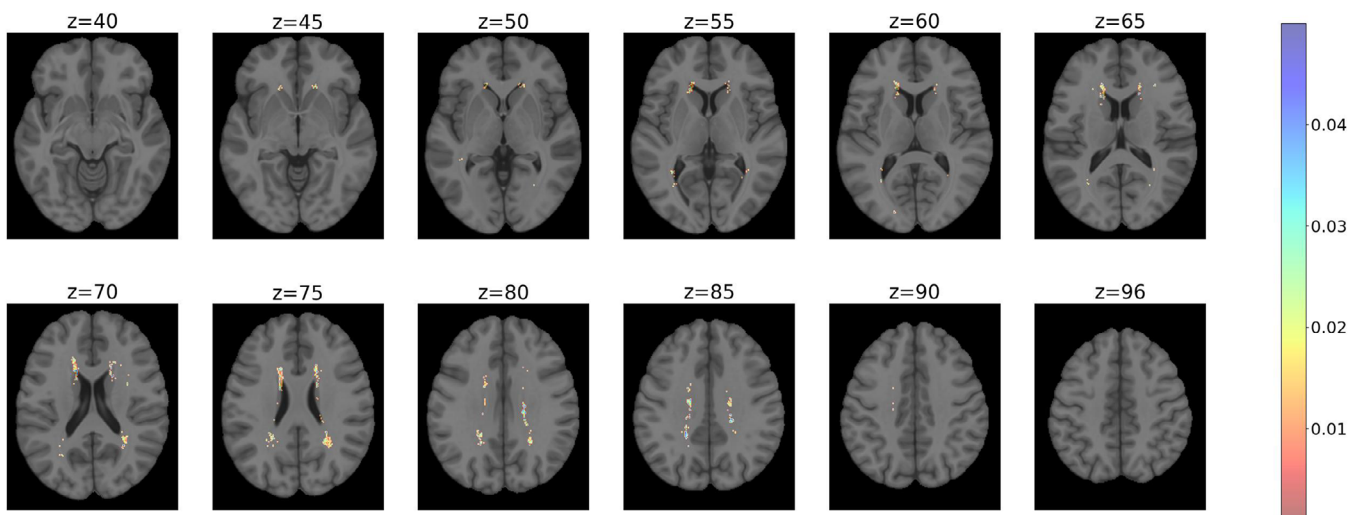
the temporal, parietal, and occipital areas.¹² Other factors, such as genetic mutations, which could contribute to WMH increase in these areas, might help to explain these contradictory results. In addition, U-fibers, which are spared in vascular disease, also connected cortical regions within ventral networks.³⁹ This could also explain this negative result.

Distinct patterns of voxel- and connection-based WMH distributions in EOAD and LOAD were underlined by different extents of contribution from amyloid or vascular risk factors. The restricted distribution in the occipital region, tracts, and visual network in EOAD may reflect the dominant influence of amyloid independent of vascular risk factors, in line with one previous genetic EOAD study that reported increased WMH burden surrounding occipital region.⁴⁰ In contrast, the widespread WMH distributions in LOAD could indicate the interplay of both amyloid and vascular risk factors. This is consistent with a study focused on pre-dementia populations, which found two components

Amyloid level



Hypertension



Smoking

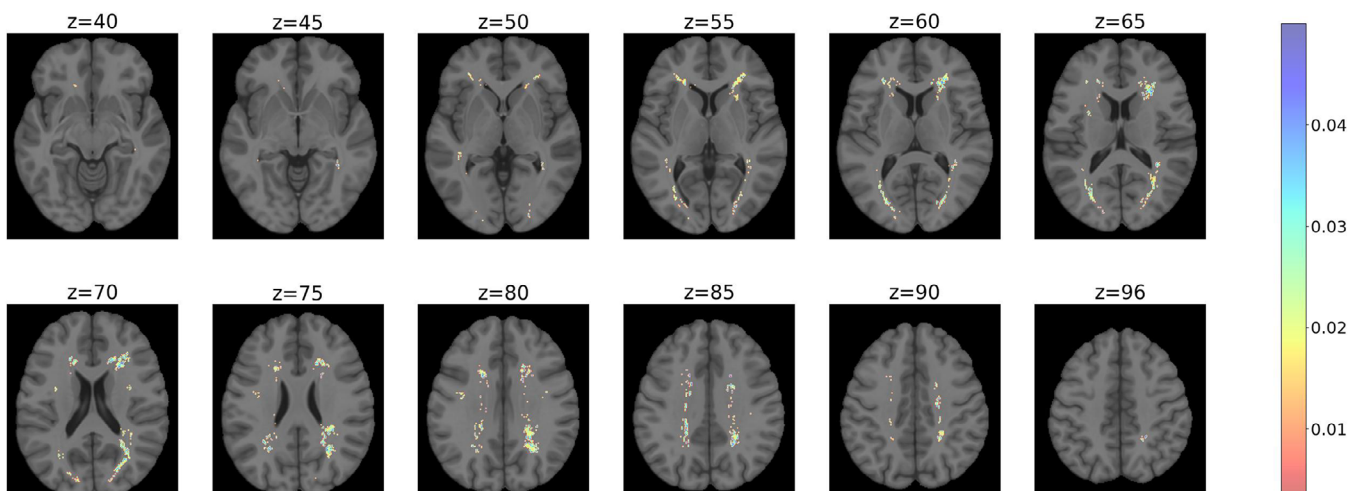


FIGURE 4 The effect of amyloid and vascular risk factors on the voxel-based white matter hyperintensity (WMH) distribution. Note: only significant results and voxels with $p < 0.05$ were shown.

TABLE 3 Association of PC1 of streamlines passing through WMH in each tract with amyloid and vascular risk factors.

	Early onset	Late onset
Amyloid	0.19*	0.19***
Diabetes	0.06	-0.04
HTN	0.04	0.18***
HL	-0.04	0.01
IHD	NA	-0.03
Smoking	0.01	0.16**

Abbreviations: HTN, hypertension; HL, hyperlipidemia; IHD, ischemic heart disease; PC1, first principal component.

Note: Models were adjusted for age and sex, *p*-values were labeled as: *0.01–0.05, **0.001–0.01, *** < 0.001, 0.05–0.1.

of WMHs, suggesting the existence of both vascular-dependent and vascular-independent manifestations of WMHs.²²

4.1 | Limitations

The limitation of this study is that both 2D FLAIR and 3D FLAIR images were included for WMH analysis. Compared with 3D FLAIR, 2D FLAIR could have missed small WMH lesions in-between the slices and thus underestimate their impact on the network connectivity. However, including both sets of images was essential to maintain an adequate sample size. Furthermore, the diagnosis of AD necessitates both patho-

logical confirmation of positive amyloid levels and clinical diagnosis of dementia,⁴¹ making it difficult to separate the effects of amyloid from dementia in group comparisons.

5 | CONCLUSION

We explored the distinct patterns of WMH distribution in both voxel-based and connection-based levels in EOAD and LOAD, and we investigated their associated etiologies. Our findings indicate that EOAD displayed a more restricted pattern of WMH distribution, likely attributed to amyloid accumulation. Conversely, LOAD showed more widespread WMH distribution patterns, which were associated with both amyloid and vascular risk factors. Our study suggests the potential need for different treatment approaches to WMH in EOAD and LOAD.

ACKNOWLEDGMENTS

The authors have nothing to report. This work was supported by the National Natural Science Foundation of China (Grant No. 81971577 & 82271936).

CONSENT STATEMENT

The ADNI database used in this study was approved by institutional review boards of all participating institutions, and written informed consent was obtained from all participants.

TABLE 4 Association of WMH connected networks with amyloid and vascular risk factors.

	Amyloid	Diabetes	HTN	HL	IHD	Smoking
Early onset						
Global	0.20*	0.17	-0.12	-0.03	NA	-0.08
Default mode	0.1	-0.12	0.07	0.04	NA	-0.16
Dorsal attention	0.11	0	-0.08	0.1	NA	-0.13
Fronto-parietal	0.15	0.09	0	-0.1	NA	-0.05
Limbic	-0.18	0	-0.04	0	NA	-0.09
Somatomotor	0.18	0.09	0.06	-0.12	NA	-0.09
Ventral attention	0.08	0.1	-0.27*	-0.03	NA	-0.04
Visual	0.32**	0.05	-0.05	0.1	NA	-0.04
Late onset						
Global	0.25***	0	0.16**	-0.01	-0.05	0.18**
Default mode	0.17**	0	0.06	0.02	-0.06	0.22***
Dorsal attention	0.13*	-0.02	0.08	0.04	-0.09	0.14*
Fronto-parietal	0.21***	-0.02	0.19**	0.04	-0.08	0.14*
Limbic	-0.16**	0.02	0.12*	0	-0.01	-0.08
Somatomotor	0.27***	-0.08	0.12*	-0.07	-0.06	0.10
Ventral attention	-0.04	0.07	-0.12*	-0.03	0.01	0.03
Visual	0.32***	-0.03	0.11*	-0.07	-0.01	0.13*

Abbreviations: HTN, hypertension; HL, hyperlipidemia; IHD, ischemic heart disease.

Note: Models were adjusted for age and sex, *p* values were labeled as: *0.01–0.05, **0.001–0.01, *** < 0.001, 0.05–0.1.

CONFLICT OF INTEREST STATEMENT

All authors declare no conflicts of interest.

ORCID

Hui Hong  <https://orcid.org/0000-0003-2084-203X>

REFERENCES

1. Ayodele T, Rogaeva E, Kurup JT, Beecham G, Reitz C. Early-onset Alzheimer's disease: what is missing in research? *Curr Neurol Neurosci Rep.* 2021;21:1-10.
2. Schell M, Ossenkoppele R, Strandberg O, et al. Distinct 18F-AV-1451 tau PET retention patterns in early- and late-onset Alzheimer's disease. *Brain.* 2017;140:2286-2294.
3. Palasí A, Gutiérrez-Iglesias B, Alegret M, et al. Differentiated clinical presentation of early and late-onset Alzheimer's disease: is 65 years of age providing a reliable threshold? *J Neurol.* 2015;262:1238-1246.
4. Mendez MF. Early-onset Alzheimer disease. *Neurol Clin.* 2017;35:263-281.
5. Filippi M, Basaia S, Canu E, et al. Brain network connectivity differs in early-onset neurodegenerative dementia. *Neurology.* 2017;89:1764-1772.
6. Joubert S, Gour N, Guedj E, et al. Early-onset and late-onset Alzheimer's disease are associated with distinct patterns of memory impairment. *Cortex.* 2016;74:217-232.
7. Wardlaw JM, Valdés Hernández MC, Muñoz-Maniega S. What are white matter hyperintensities made of? Relevance to vascular cognitive impairment. *J Am Heart Assoc.* 2015;4:e001140.
8. Alber J, Alladi S, Bae H-J, et al. White matter hyperintensities in vascular contributions to cognitive impairment and dementia (VCID): knowledge gaps and opportunities. *TRCI.* 2019;5:107-117.
9. Lee S, Viqar F, Zimmerman ME, et al. White matter hyperintensities are a core feature of Alzheimer's disease: evidence from the dominantly inherited Alzheimer network. *Ann Neurol.* 2016;79:929-939.
10. Young VG, Halliday GM, Kril JJ. Neuropathologic correlates of white matter hyperintensities. *Neurology.* 2008;71:804-811.
11. Arfanakis K, Evia AM, Leurgans SE, et al. Neuropathologic correlates of white matter hyperintensities in a community-based cohort of older adults. *J Alzheimer's Dis.* 2020;73:333-345.
12. Garnier-Crussard A, Cotton F, Krolak-Salmon P, Chételat G. White matter hyperintensities in Alzheimer's disease: beyond vascular contribution. *Alzheimer's & Dementia.* 2023.
13. Wardlaw JM, Allerhand M, Doubal FN, et al. Vascular risk factors, large-artery atheroma, and brain white matter hyperintensities. *Neurology.* 2014;82:1331-1338.
14. Graff-Radford J, Arenaza-Urquijo EM, Knopman DS, et al. White matter hyperintensities: relationship to amyloid and tau burden. *Brain.* 2019;142:2483-2491.
15. Moscoso A, Rey-Bretal D, Silva-Rodríguez J, et al. White matter hyperintensities are associated with subthreshold amyloid accumulation. *Neuroimage.* 2020;218:116944.
16. Gaubert M, Lange C, Garnier-Crussard A, et al. Topographic patterns of white matter hyperintensities are associated with multimodal neuroimaging biomarkers of Alzheimer's disease. *Alzheimer's res ther.* 2021;13:1-11.
17. Phuah C-L, Chen Y, Strain JF, et al. Association of data-driven white matter hyperintensity spatial signatures with distinct cerebral small vessel disease etiologies. *Neurology.* 2022;99:e2535.
18. Shirzadi Z, Schultz SA, Yau W-YW, et al. Etiology of white matter hyperintensities in autosomal dominant and sporadic Alzheimer disease. *JAMA Neurol.* 2023;80:1353-1363.
19. Jung K-H, Stephens KA, Yochim KM, et al. Heterogeneity of cerebral white matter lesions and clinical correlates in older adults. *Stroke.* 2021;52:620-630.
20. Gronewold J, Jokisch M, Schramm S, et al. Periventricular rather than deep white matter hyperintensities mediate effects of hypertension on cognitive performance in the population-based 1000BRAINS study. *J Hypertens.* 2022;40:2413.
21. Veldsman M, Kindalova P, Husain M, Kosmidis I, Nichols TE. Spatial distribution and cognitive impact of cerebrovascular risk-related white matter hyperintensities. *NeuroImage: Clin.* 2020;28:102405.
22. Lorenzini L, Ansems LT, Lopes Alves I, et al. Regional associations of white matter hyperintensities and early cortical amyloid pathology. *Brain Commun.* 2022;4:fcac150.
23. Saxena S, Keser Z, Rorden C, et al. Disruptions of the human connectome associated with hemispatial neglect. *Neurology.* 2022;98:e107-e114.
24. Salvalaggio A, Pini L, Gaiola M, et al. White matter tract density index prediction model of overall survival in Glioblastoma. *JAMA Neurol.* 2023;80:1222-1231.
25. Royse SK, Minhas DS, Lopresti BJ, et al. Validation of amyloid PET positivity thresholds in centiloids: a multisite PET study approach. *Alzheimer's res ther.* 2021;13:99.
26. Avants BB, Tustison N, Song G. Advanced normalization tools (ANTS). *Insight j.* 2009;2:1-35.
27. Isensee F, Schell M, Pflueger I, et al. Automated brain extraction of multisequence MRI using artificial neural networks. *Hum Brain Mapp.* 2019;40:4952-4964.
28. Billot B, Greve DN, Puonti O, et al. SynthSeg: domain randomisation for segmentation of brain scans of any contrast and resolution. *arXiv preprint.* 2021. arXiv:210709559.
29. Mojiri Forooshani P, Biparva M, Ntiri EE, et al. *Deep Bayesian Networks for Uncertainty Estimation and Adversarial Resistance of White Matter Hyperintensity Segmentation.* Wiley Online Library; 2022.
30. Woolrich MW, Jbabdi S, Patenaude B, et al. Bayesian analysis of neuroimaging data in FSL. *Neuroimage.* 2009;45:S173-S186.
31. Yeh F-C. Population-based tract-to-region connectome of the human brain and its hierarchical topology. *Nat Commun.* 2022;13:4933.
32. Glasser MF, Coalson TS, Robinson EC, et al. A multi-modal parcellation of human cerebral cortex. *Nature.* 2016;536:171-178.
33. Yeo BT, Krienen FM, Sepulcre J, et al. The organization of the human cerebral cortex estimated by intrinsic functional connectivity. *J Neurophysiol.* 2011.
34. McAleese KE, Walker L, Graham S, et al. Parietal white matter lesions in Alzheimer's disease are associated with cortical neurodegenerative pathology, but not with small vessel disease. *Acta Neuropathol.* 2017;134:459-473.
35. Bozzali M, Falini A, Franceschi M, et al. White matter damage in Alzheimer's disease assessed in vivo using diffusion tensor magnetic resonance imaging. *J Neurol Neurosurg Psychiatry.* 2002;72:742.
36. Brun A, Englund E. A white matter disorder in dementia of the Alzheimer type: a pathoanatomical study. *Ann Neurol.* 1986;19:253-262.
37. Webb AJ, Werring DJ. New insights into cerebrovascular pathophysiology and hypertension. *Stroke.* 2022;53:1054-1064.
38. Koohi F, Harshfield EL, Markus HS. Contribution of conventional cardiovascular risk factors to brain white matter hyperintensities. *J Am Heart Assoc.* 2023;12:e030676.
39. Kalari RN, Erkinjuntti T. Small vessel disease and subcortical vascular dementia. *J Clin Neurosci.* 2006;2:1-11.
40. Mao C, Li J, Huang X, et al. White matter hyperintensities and patterns of atrophy in early onset Alzheimer's disease with causative gene mutations. *Clin Neurol Neurosurg.* 2021;203:106552.
41. Jack Jr CR, Albert MS, Knopman DS, et al. Introduction to the recommendations from the National Institute on Aging-Alzheimer's Association workgroups on diagnostic guidelines for Alzheimer's disease. *Alzheimer Dement.* 2011;7:257-262.

SUPPORTING INFORMATION

Additional supporting information can be found online in the Supporting Information section at the end of this article.

How to cite this article: Hong H, Chen Y, Liu W, Luo X, Zhang M; for the Alzheimer's Disease Neuroimaging Initiative (ADNI). Distinct patterns of voxel- and connection-based white matter hyperintensity distribution and associated factors in early-onset and late-onset Alzheimer's disease. *Alzheimer's Dement.* 2024;16:e12585.
<https://doi.org/10.1002/dad2.12585>